

Cite this: *Energy Environ. Sci.*,  
2020, 13, 238

# Efficient hydrogen peroxide synthesis by metal-free polyterthiophene *via* photoelectrocatalytic dioxygen reduction†

Wenjun Fan,<sup>ab</sup> Bingqing Zhang,<sup>ab</sup> Xiaoyu Wang,<sup>c</sup> Weiguang Ma,<sup>id a</sup> Deng Li,<sup>a</sup> Zhiliang Wang,<sup>a</sup> Michel Dupuis,<sup>id c</sup> Jingying Shi,<sup>id \*a</sup> Shijun Liao<sup>id \*b</sup> and Can Li<sup>id \*a</sup>

Solar hydrogen peroxide (H<sub>2</sub>O<sub>2</sub>) produced through the selective two-electron (2e<sup>-</sup>) oxygen reduction pathway is an ideal alternative to liquid fuel in addition to being a versatile chemical. Up to now, low photocatalytic activity, low selectivity and serious competing reactions have been big hurdles in the production of solar H<sub>2</sub>O<sub>2</sub> in an efficient way. Herein, we report that polyterthiophene (pTTh), a metal-free narrow-bandgap polymeric semiconductor, is an efficient photocathode for H<sub>2</sub>O<sub>2</sub> production in alkaline solution. We found that 2e<sup>-</sup> selectivity for the ORR is dependent on the pH of electrolytes and approaches 100% at pH ~ 13. A record-high H<sub>2</sub>O<sub>2</sub> concentration of 110 mmol L<sup>-1</sup> is achieved, which is two orders of magnitude higher than the previous photosynthesized H<sub>2</sub>O<sub>2</sub>. Furthermore, NiFeO<sub>x</sub>/BiVO<sub>4</sub>-pTTh dual-photoelectrodes in photoelectrochemical devices enabled bias-free synthesis of solar H<sub>2</sub>O<sub>2</sub> of concentration ~90 mmol L<sup>-1</sup> for several cycles without any noticeable decay. This extremely high 2e<sup>-</sup> selectivity is attributed to the intrinsic electrochemical properties of pTTh. Theoretical calculations suggested that the selectivity-determining step in the 2e<sup>-</sup> process is over ~200 times faster than that in the 4e<sup>-</sup> pathway. Our work paves an alternative way of generating liquid solar fuel that is very promising for practical applications.

Received 15th July 2019,  
Accepted 20th November 2019

DOI: 10.1039/c9ee02247c

rsc.li/ees

## Broader context

The importance of hydrogen peroxide (H<sub>2</sub>O<sub>2</sub>) has been witnessed by its annual production, approaching 6 million tons in 2016. However, this otherwise highly versatile and green chemical is currently manufactured by the energy-intensive anthraquinone process, which requires complex and large-scale infrastructure. In this regard, H<sub>2</sub>O<sub>2</sub> production from solar energy is an ideal way, in which only water, oxygen and sunlight (H<sub>2</sub>O + 1/2O<sub>2</sub> → H<sub>2</sub>O<sub>2</sub>, ΔG = 117 kJ mol<sup>-1</sup>) are required. Nevertheless, all previously reported particulate photocatalytic systems suffered from poor efficiency in H<sub>2</sub>O<sub>2</sub> generation, due to the serious back reaction by photogenerated holes and the low selectivity of the two-electron (2e<sup>-</sup>) pathway. In our contribution, we propose a selective metal-free polyterthiophene photocathode combined with a spatially separated photoelectrochemical cell to generate a record high H<sub>2</sub>O<sub>2</sub> concentration of 110 millimole per liter (mM). Our work provides an attractive route for the practical synthesis of liquid solar fuel.

## Introduction

Solar fuel production has attracted increasing attention as the key technology to relieve environmental issues and reduce the reliance on fossil resources.<sup>1,2</sup> Substantial efforts have focused on the generation of hydrogen (from overall water splitting) and carbonaceous fuels like methanol (from CO<sub>2</sub> reduction) by conversion of solar energy.<sup>3-6</sup> In contrast, another type of solar fuel, hydrogen peroxide (H<sub>2</sub>O<sub>2</sub>), has received less attention so far.<sup>7</sup> Generally, H<sub>2</sub>O<sub>2</sub> could be synthesized *via* photo(electro)catalytic H<sub>2</sub>O oxidation or O<sub>2</sub> reduction following a selective two-electron (2e<sup>-</sup>) pathway.<sup>8-11</sup> This is the reason why we also call it as one of the solar fuels. Similar to H<sub>2</sub> in a H<sub>2</sub>-O<sub>2</sub> fuel cell, H<sub>2</sub>O<sub>2</sub> can also be

<sup>a</sup> State Key Laboratory of Catalysis, Dalian National Laboratory for Clean Energy, Dalian Institute of Chemical Physics, Chinese Academy of Sciences, Dalian 116023, Liaoning, China. E-mail: jingyingshi@dicp.ac.cn, canli@dicp.ac.cn

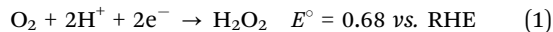
<sup>b</sup> The Key Laboratory of Fuel Cell Technology of Guangdong Province & The Key Laboratory of New Energy Technology of Guangdong University, School of Chemistry and Chemical Engineering, South China University of Technology, Guangzhou, 510641, Guangdong, China. E-mail: chsjliao@scut.edu.cn

<sup>c</sup> Department of Chemical and Biological Engineering, University at Buffalo, State University of New York Buffalo, NY 14260, USA

† Electronic supplementary information (ESI) available. See DOI: 10.1039/c9ee02247c

utilized for electricity generation in a single-compartment  $\text{H}_2\text{O}_2$  fuel cell with a theoretical output voltage of above 1.09 V.<sup>12</sup> Besides, it is a value-added chemical which has been extensively applied in organic synthesis, pulp bleaching, waste-water treatment and medical disinfection. Meanwhile, it exists in a liquid state at normal temperature and pressure that makes it convenient for storage, transportation, and compatibility with the current energy infrastructure.<sup>13</sup> Hence,  $\text{H}_2\text{O}_2$  is an ideal solar fuel that deserves increased research.

However, the synthesis of solar  $\text{H}_2\text{O}_2$  has been extremely challenging up to now. The solar water oxidation reaction (WOR) itself is rather difficult to realize due to the uphill thermodynamics (1.76 V) together with sluggish kinetics.<sup>10,14</sup> Besides, the as-synthesized  $\text{H}_2\text{O}_2$  can readily decompose at a highly oxidative photoanode because the  $\text{H}_2\text{O}_2$  molecule is an excellent hole scavenger.<sup>15</sup> Several photoanodes, such as  $\text{BiVO}_4$  and  $\text{WO}_3$ ,<sup>10,16,17</sup> combined with highly concentrated hydrogen carbonate solution as an electrolyte have been reported, but the formed  $\text{H}_2\text{O}_2$  is not more than 5 millimole per liter ( $\text{mmol L}^{-1}$ ) *via* the photoelectrocatalytic WOR. Alternatively, solar  $\text{H}_2\text{O}_2$  can be obtained from an oxygen reduction reaction (ORR) *via* a  $2e^-$  pathway (eqn (1) under acidic conditions and eqn (2) under alkaline conditions), which is enabled by applying the particulate system or a photoelectrochemical (PEC) cell with a photocathode.



For instance, various photocatalysts such as inorganic  $\text{ZnO}$ ,  $\text{TiO}_2$ , and  $\text{CdS}$  and organic  $g\text{-C}_3\text{N}_4$  have been found to be active for the artificial photosynthesis of  $\text{H}_2\text{O}_2$  in a particulate system.<sup>18–21</sup> Nevertheless, the achieved concentration is limited to a rather low level of a few  $\text{mmol L}^{-1}$ , which is due to the following facts: (1) the produced  $\text{H}_2\text{O}_2$  is susceptible to a back reaction of reoxidation by holes, (2) low activity and selectivity for the  $2e^-$  process. Thus, most of the photocatalytic  $\text{H}_2\text{O}_2$  generation approaches rely on the use of sacrificial reagents (*e.g.* alcohol, formic acid and formate) which are intrinsically thermodynamic down-hill processes, and therefore solar energy cannot be stored in the form of chemicals.

In contrast, PEC cells with spatially separated two half-reactions and isolated electrolytes offer solutions to address the loss of  $\text{H}_2\text{O}_2$  from the rapid back reaction. The  $\text{H}_2\text{O}_2$  generation from PEC cells started with the seminal work of the Eric Daniel Głowacki group using a hydrogen-bonded organic semiconductor as the photocathode, although only  $3 \text{ mmol L}^{-1}$  was accumulated.<sup>22</sup> Subsequently, a  $2e^-$  ORR electrocatalyst was wired with a  $\text{WO}_3$  photoanode as the driving force and a high concentration of  $48 \text{ mmol L}^{-1}$  was achieved in a catholyte after a long illumination duration of 24 h.<sup>23</sup> However, to date, very few semiconducting materials have been found to be active for the PEC ORR and thus high-yield synthesis of  $\text{H}_2\text{O}_2$  *via* a selective photoelectrocatalytic ORR has not been reported.

Polymeric semiconductors have emerged as a class of promising materials for energy-related conversions. They offer the advantages of low-cost, facile synthesis and broad light absorption.<sup>24</sup>

As a p-type polymeric semiconductor material, polyterthiophene (pTTh) has been identified to be an active photocathode for the ORR in  $\text{H}_2\text{-O}_2$  fuel cells and biofuel cells by our group and other groups.<sup>25–27</sup> However, the  $2e^-$  selectivity of the pTTh photocathode for the ORR has not been investigated. In the present work, we found that the ORR  $2e^-$  selectivity of pTTh is strongly dependent on the pH of the electrolytes and it reaches nearly 100% at  $\text{pH} \sim 13$  without the requirement of any other additives or cocatalysts. We observed that a concentration of solar  $\text{H}_2\text{O}_2$  of  $\sim 110 \text{ mmol L}^{-1}$  can be achieved, which is by far the most concentrated  $\text{H}_2\text{O}_2$  derived *via* artificial photosynthesis methods.<sup>28</sup> Furthermore, by wiring a pTTh photocathode with a  $\text{NiFeO}_x/\text{BiVO}_4$  photoanode, the as-fabricated dual-photoelectrode device was capable of self-driven preparation of high-concentration  $\text{H}_2\text{O}_2$  for several cycles without any noticeable decay. The high selectivity of the  $2e^-$  ORR was investigated by electrochemical experiments and density functional theory calculations. Our work sets an example for artificial photosynthesis of  $\text{H}_2\text{O}_2$  with high yield, indicating that  $\text{H}_2\text{O}_2$  may be a very promising liquid solar fuel to be developed.

## Results and discussion

### Characterization of the pTTh photoelectrode

Polyterthiophene (pTTh) films were deposited on three-dimensional carbon paper (CP) or smooth glassy carbon (GC) by electropolymerization of terthiophene. The corresponding photoelectrodes are denoted as pTTh/CP and pTTh/GC for convenience.<sup>29</sup> As shown in Fig. 1a, diffuse reflectance UV-vis spectrum of the pTTh/CP electrode exhibits wide absorption extending to 640 nm. The bandgap of pTTh is estimated to be *ca.* 2.0 eV from the Tauc plot (Fig. S1, ESI†). The red-brown photoelectrode (Fig. 1a, inset) appears with a flower-like morphology assembled in ultrathin nanosheets (Fig. 1b) as revealed by SEM observation. Notably, the nanoporous structure facilitates the immediate transport of the photogenerated excitons to the polymer-solution interface and their participation in the redox reaction while suppressing the undesirable electron-hole recombination.<sup>30</sup> Cyclic voltammetry (CV) measurements were used to evaluate the HOMO and LUMO energy levels – from the ionization potential and the electron affinity, respectively – and determine the bandgap of pTTh (Fig. S2a and b, ESI†). A careful analysis of the CVs of the

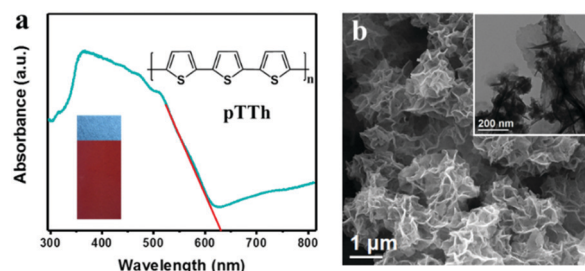


Fig. 1 (a) UV-vis diffuse reflectance spectrum of pTTh; the inset shows the molecular structure and the digital photo of the as-prepared pTTh electrode, respectively. (b) SEM image of the pTTh film; the inset shows the TEM image of the pTTh film.

material (zoom at lower current, Fig. S2b, ESI†) revealed that the onset of oxidation occurred at *ca.* 0.39 V. The corresponding HOMO energy level was calculated to be  $-5.13$  eV (using the formula given in the ESI†), and the LUMO energy was  $-3.13$  eV by adding the optical bandgap ( $E_g$ ) to the calculated HOMO energy level. Thus, LUMO and HOMO potentials are calculated to be  $-1.37$  V and  $0.63$  V, respectively. To obtain more information of the electronic structure, a Mott–Schottky (M–S) analysis was performed on the pTTh/GC electrode (Fig. S2c, ESI†). The M–S plot exhibits a negative slope, which is typical for p-type semiconductors. The flat band potential locates at *ca.* 0.48 V vs. NHE at pH 13; thus, the conduction band energy level (LUMO level equivalent) is estimated to be *ca.*  $-1.42$  V, similar to the energy level results of the CVs. Notably, it is thermodynamically favorable for both the oxygen reduction reaction (either  $4e^-$  or  $2e^-$  pathway) and the hydrogen evolution reaction. Control experiments were conducted on a rotating-ring disk system (Fig. S3, ESI†) to check the PEC activity of pTTh toward the ORR in 0.1 M KOH solution under  $100 \text{ mW cm}^{-2}$  light illumination. Remarkably, a pronounced photocurrent was detected in the  $\text{O}_2$ -saturated electrolyte in contrast to a negligible photocurrent in the  $\text{Ar}$ -saturated electrolyte (Fig. S4 and S5, ESI†), suggesting that the ORR is the dominant photocathodic process.

### pH-Dependent photocathodic ORR to $\text{H}_2\text{O}_2$

ORR performance is commonly affected by the pH of solutions since it is a proton-coupled electron transfer process.<sup>31</sup> To unravel the pH-dependence of the PEC ORR activity of the pTTh photocathode, linear sweep voltammetry (LSV) curves of the pTTh/GC in  $\text{O}_2$ -saturated electrolytes with different pH values were investigated. It can be seen that the photocurrent density is remarkably enhanced with a negative shift of the applied bias for all curves (Fig. 2a). Meanwhile, under the same applied bias, the photocurrent density gradually increases with the increase of pH. In other words, pTTh shows higher PEC ORR activity in alkaline electrolytes than in acidic electrolytes. To demonstrate the pH-dependence more directly, the photocurrent densities at specific applied potentials of 0.6, 0.7 and 0.8 V are plotted together with the onset potentials derived from Fig. 2a with respect to the corresponding pH. As shown in Fig. 2b, it can be seen that both the photocurrent and the onset

potential depend greatly on the pH of the solutions. For example, under the bias of 0.6 V, the photocurrent increases from less than  $-0.2 \text{ mA cm}^{-2}$  at pH 0.1 to about  $-1.7 \text{ mA cm}^{-2}$  at pH 12.9. And the largest shift of the onset potential is as high as 0.48 V (0.67 V at pH 0.1 and 1.15 V at pH 12.9). The pH of the electrolyte is thus found to be a key parameter to regulate the PEC ORR activity of the pTTh photocathode.

The selectivity for  $\text{H}_2\text{O}_2$  generation and its pH-dependence for the pTTh photocathode were investigated by the conventional rotating ring-disk electrode (RRDE) technique (see ESI† Methods). Fig. 3a exhibits the disk current for the ORR and ring current for the  $\text{H}_2\text{O}_2$  oxidation reaction in 0.1 M KOH solution. The onset potentials at the ring and the disc coincide at  $\sim 1.25$  V. As the overpotential increases, most of the current in the disc can be accounted for by the amount of  $\text{H}_2\text{O}_2$  detected at the ring (dashed-dotted line in Fig. 3a). The  $\text{H}_2\text{O}_2$  selectivity with pTTh exceeds 95% in the wide potential range of 0.2 to 1.2 V (Fig. 3b), suggesting that the PEC ORR on pTTh is dominated by a  $2e^-$  process with  $\text{HO}_2^-$  as the final product in alkaline solution (pH 12.9). By contrast, the  $\text{H}_2\text{O}_2$  selectivity gradually decreases with decreasing pH (Fig. 3c) that only maintains  $\sim 50\%$  in strong acidic solution (pH 0.1). Thus, it can be concluded that both the PEC activity and  $\text{H}_2\text{O}_2$  selectivity of pTTh for the ORR extremely depend on the pH of electrolytes. In view of the superior activity and selectivity for the  $2e^-$  ORR to  $\text{H}_2\text{O}_2$  in 0.1 M KOH solution (pH 12.9), the discussion hereafter corresponds to these conditions with saturated  $\text{O}_2$  unless otherwise stated ( $\text{HO}_2^-$  is the deprotonated anion of  $\text{H}_2\text{O}_2$  in alkaline media; we will use  $\text{H}_2\text{O}_2$  and  $\text{HO}_2^-$  interchangeably throughout this work).

To reveal the ORR kinetics of the material, the rotating disk electrode (RDE) measurements were recorded. As shown in

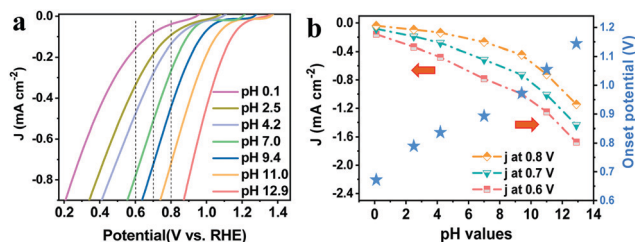


Fig. 2 (a) LSVs of the pTTh electrode measured in  $\text{O}_2$ -saturated electrolytes with different pH values under 1 sun illumination. Rotation rate: 1600 rpm. Ionic strength is constant at 0.1 M. (b) Correlation between current densities of the ORR at 0.6, 0.7 and 0.8 V vs. RHE and the pH values (dotted-dashed lines); correlation between onset potentials (at  $0.1 \text{ mA cm}^{-2}$ ) and the pH values (blue stars).

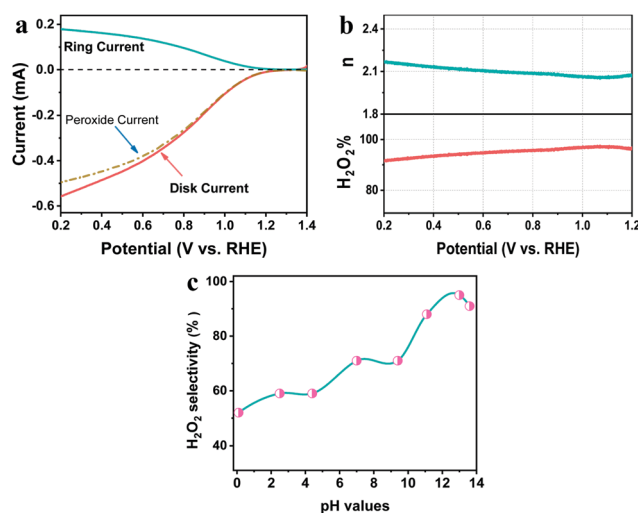


Fig. 3 (a) RRDE voltammograms of pTTh in  $\text{O}_2$  saturated solution at pH 12.9 under 1 sun illumination with the disc current, ring current and current corresponding to hydrogen peroxide obtained from the ring current. The disk potential was scanned at  $10 \text{ mV s}^{-1}$  and the ring potential was constant at 1.5 V vs. RHE. (b) Percentage of peroxide and the electron transfer number ( $n$ ) of pTTh at various potentials, calculated from RRDE data. (c) pH dependent hydrogen peroxide selectivity of pTTh calculated by RRDE results.

Fig. S6 (ESI<sup>†</sup>), the linearity of the Koutecky–Levich (K–L) plot and near parallelism of the fitting lines over the investigated potential range suggest a first-order reaction kinetics for the ORR with respect to the concentration of dissolved O<sub>2</sub> and similar electron transfer numbers at different potentials (Fig. S6b, ESI<sup>†</sup>).<sup>32</sup> Meanwhile, the electron-transfer number (*n*) is calculated to be approximately 2.0 from the slopes of K–L plots, which agrees well with the above RRDE results. According to the Levich equation (for details see ESI<sup>†</sup>, Methods), the diffusion-limited current density is calculated to be 2.19 mA cm<sup>-2</sup> (2e<sup>-</sup> pathway) or 4.39 mA cm<sup>-2</sup> (4e<sup>-</sup> pathway) at 1600 rpm.<sup>33</sup> At 0.4 V, the polarization curve reaches a current density (*ca.* 2.0 mA cm<sup>-2</sup>) close to the limiting value of H<sub>2</sub>O<sub>2</sub> formation, which implies the fast kinetics of the pTTh photocathode toward the 2e<sup>-</sup> pathway. Therefore, the combined characterization of RRDE and RDE measurements clearly predicted an efficient synthesis of H<sub>2</sub>O<sub>2</sub> by the PEC method on the pTTh photocathode in alkaline solution.

### PEC H<sub>2</sub>O<sub>2</sub> production from the pTTh photocathode

To study the synthesis of H<sub>2</sub>O<sub>2</sub> *via* the PEC ORR, the pTTh/CP was used as the photocathode in a three-electrode configuration with 0.1 M KOH as the electrolyte. A Nafion membrane was used to isolate the anolyte from the O<sub>2</sub>-saturated catholyte in order to prevent the reoxidation of the generated H<sub>2</sub>O<sub>2</sub> by the anode.<sup>22</sup> An external bias of 0.65 V was applied on the pTTh under simulated 100 mW cm<sup>-2</sup> illumination. Considering that H<sub>2</sub>O<sub>2</sub> is susceptible to temperature and UV irradiation, we conducted control experiments to determine the synthesis conditions (Fig. S7, ESI<sup>†</sup>), in which 100 mmol L<sup>-1</sup> H<sub>2</sub>O<sub>2</sub> in 0.1 M KOH solution was investigated as an example. It can be seen that H<sub>2</sub>O<sub>2</sub> scarcely decomposed in the temperature range of 10–30 °C even after 24 h. Under UV-filtered illumination ( $\lambda > 420$  nm), more than 90% of H<sub>2</sub>O<sub>2</sub> was retained even when the exposure duration was longer than 20 h. In contrast, the extended wavelength illumination (full spectrum) caused 90% loss within 16 h. During the UV irradiation, the bond between hydrogen and oxygen would cleave and induce a chain reaction according to the Haber–Weiss reaction theory,<sup>34</sup> which would lead to the violet decomposition of H<sub>2</sub>O<sub>2</sub>. With these combined observations, the reaction temperature was maintained at 20 °C with applied visible light irradiation as the light source.

Fig. 4a shows the time courses of H<sub>2</sub>O<sub>2</sub> production at the cathodic side. It can be seen that the concentration of H<sub>2</sub>O<sub>2</sub> increased to 80 mmol L<sup>-1</sup> almost linearly within 5 h and an even higher concentration of 110 mmol L<sup>-1</sup> was achieved after a sustained PEC reaction for 11 h despite a slight slowing down of the growth rate. The time courses of faradaic efficiency for H<sub>2</sub>O<sub>2</sub> synthesis (Fig. 4a, green) suggest an efficiency of above 90% over the entire time range. In comparison with the previous photosynthesized H<sub>2</sub>O<sub>2</sub>, the produced H<sub>2</sub>O<sub>2</sub> in this work achieved a record high concentration which is *ca.* two orders of magnitude greater than the previous results (Table S1, ESI<sup>†</sup>). Concerning the solar H<sub>2</sub>O<sub>2</sub> synthesis *via* direct photocathodic ORR, the generation rate of H<sub>2</sub>O<sub>2</sub> (10 mmol L<sup>-1</sup> h<sup>-1</sup>) is four orders of magnitude higher than that derived on an

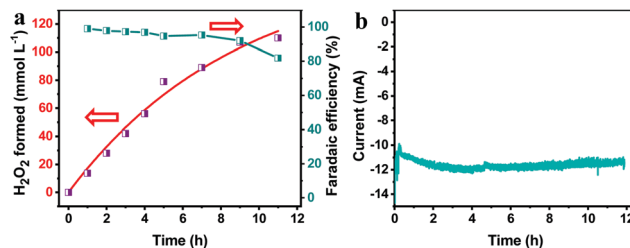


Fig. 4 (a) Time course for H<sub>2</sub>O<sub>2</sub> accumulation with the pTTh photocathode (9 cm<sup>2</sup>) and corresponding faradaic efficiency. The green line shows the faradaic efficiency. The red line is the fitting results using the equation  $[H_2O_2] = (K_f/K_d)[1 - \exp(-K_d t)]$ . (b) The corresponding *I*–*t* curve measured at 0.65 V (vs. RHE) of pTTh for ORR. Electrolyte: 0.1 M KOH; illumination: 100 mW cm<sup>-2</sup> Xe lamp with a solar simulator; counter electrode: Pt; reference electrode: SCE.

organic pigment photocathode in acidic solution (3 mmol L<sup>-1</sup> in 50 h, *i.e.* 0.06 mmol L<sup>-1</sup> h<sup>-1</sup>).<sup>22</sup> Meanwhile, the generated current stayed almost constant within the whole testing duration as shown in Fig. 4b, which indicates that the parasitic reaction was boosted with the formation of H<sub>2</sub>O<sub>2</sub>.

To evaluate the competitive H<sub>2</sub>O<sub>2</sub> reduction reaction involved in the production of H<sub>2</sub>O<sub>2</sub>, the LSV curves of pTTh/CP in Ar-saturated 0.1 M KOH solution containing various concentrations of H<sub>2</sub>O<sub>2</sub> (0–100 mmol L<sup>-1</sup>) in the dark and under illumination were compared. Without exposure to light, the reduction of H<sub>2</sub>O<sub>2</sub> is almost negligible (Fig. S8a, ESI<sup>†</sup>) in spite of the concentration being as high as 100 mmol L<sup>-1</sup>. Under illumination, the photo-reduction significantly increased with the increased concentration of H<sub>2</sub>O<sub>2</sub>. In the presence of 100 mmol L<sup>-1</sup> H<sub>2</sub>O<sub>2</sub>, the photocurrent reached *ca.* –0.12 mA cm<sup>-2</sup> at a bias of 0.65 V (Fig. S8b, ESI<sup>†</sup>), accounting for only 15% of the photocurrent generated by the ORR (Fig. S8c, ESI<sup>†</sup>). This results in the consecutive accumulation of H<sub>2</sub>O<sub>2</sub> with a only slight decrease in faradaic efficiency.

In O<sub>2</sub>-saturated solution, the actual kinetics can be regarded as zero-order owing to the constant concentration of the dioxygen. For the decomposition of H<sub>2</sub>O<sub>2</sub> by the reduction reaction, it commonly follows the first-order kinetics related to the concentration of H<sub>2</sub>O<sub>2</sub> (denoted as [H<sub>2</sub>O<sub>2</sub>]). Therefore, the kinetic equation for PEC synthesis of H<sub>2</sub>O<sub>2</sub> can be expressed as

$$[H_2O_2] = (K_f/K_d)[1 - \exp(-K_d t)]$$

where *K<sub>f</sub>* is the formation rate constant, *K<sub>d</sub>* is the decomposition rate constant and *t* is the reaction time. It is clearly seen in Fig. 4a that the experimental data (purple dots) can be well fitted with the kinetic equation (red curve). Accordingly, the *K<sub>f</sub>* and *K<sub>d</sub>* were calculated to be 18.14 mmol L<sup>-1</sup> h<sup>-1</sup> and 0.11 h<sup>-1</sup>, respectively. It should be noted that the *K<sub>f</sub>* is more than ten times higher than that in previous results in H<sub>2</sub>O<sub>2</sub> preparation *via* solar-to-chemical conversion routes.<sup>19,35,36</sup> On the other hand, the *K<sub>d</sub>* remains relatively low, enabling the produced H<sub>2</sub>O<sub>2</sub> to reach a considerably high steady concentration. Furthermore, pTTh is negatively charged in 0.1 M KOH derived from the measurement of zeta-potential (Fig. S9, ESI<sup>†</sup>). This surface property may facilitate the removal of the generated HO<sub>2</sub><sup>-</sup> species on the

pTTh surface by electrostatic repulsion and thus release the active sites for a sustained reaction.

### Unbiased $\text{H}_2\text{O}_2$ production by coupling with the photoanode

The ultimate goal of photosynthetic  $\text{H}_2\text{O}_2$  production is to make efficient and stable overall unbiased  $\text{H}_2\text{O}_2$  generation devices in a cost-effective way. To demonstrate the remarkable performance of the pTTh photocathode, we constructed a bias-free overall  $\text{H}_2\text{O}_2$  production system by wiring it to a  $\text{BiVO}_4$  photoanode with a parallel illumination configuration (Fig. 5a).  $\text{BiVO}_4$  is one of the most promising photoanode materials with intriguing properties for the PEC water oxidation reaction.<sup>37,38</sup> The energy levels of  $\text{BiVO}_4$  were estimated by the UV-vis and the Mott-Schottky analysis (Fig. S10, ESI<sup>†</sup>). The schematic energy diagram and the photogenerated carrier transfer processes are presented in Fig. S11 (ESI<sup>†</sup>). Owing to the difference between the Fermi levels of the n-type  $\text{BiVO}_4$  and p-type pTTh, the PEC system produces spontaneously an interior bias between the two photoelectrodes equal to the open-circuit voltage ( $V_{\text{OC}}$ ). To facilitate the interfacial charge transfer, a thin  $\text{NiFeO}_x$  layer was photo-deposited on the  $\text{BiVO}_4$  surface as a cocatalyst (Fig. S12, ESI<sup>†</sup>).<sup>39</sup> The resulting  $\text{NiFeO}_x/\text{BiVO}_4$  photoanode exhibited a much earlier onset potential and remarkably higher photocurrent density ( $2.5 \text{ mA cm}^{-2}$ ) at 1.23 V compared with pristine  $\text{BiVO}_4$  (Fig. S13, ESI<sup>†</sup>).

Fig. 5b displays the LSV curves of the pTTh/CP photocathode and the  $\text{NiFeO}_x/\text{BiVO}_4$  photoanode in 0.1 M KOH solution and 1M potassium borate buffer, respectively. The working area of both photoelectrodes is  $9 \text{ cm}^2$  (Fig. S14, ESI<sup>†</sup>). An intersection point between the two curves corresponds to a current of 10.2 mA. This result predicts that the  $\text{NiFeO}_x/\text{BiVO}_4$ -pTTh/CP

dual-photoelectrodes in a PEC cell are able to self-drive simultaneous  $\text{H}_2\text{O}$  oxidation on the photoanode and  $\text{O}_2$  reduction on the photocathode only with light illumination,<sup>40,41</sup> although there is a pH mismatch between the photoanode and photocathode. Meanwhile, prolonged testing of the  $\text{NiFeO}_x/\text{BiVO}_4$  photoanode exhibits a stable photocurrent over 20 h under illumination (Fig. S15, ESI<sup>†</sup>). The time course for the unbiased production of  $\text{H}_2\text{O}_2$  is shown in Fig. 5c. As expected, the concentration of  $\text{H}_2\text{O}_2$  increases linearly with time and reaches the maximum  $\sim 90 \text{ mmol L}^{-1}$  after 14 h of illumination. The corresponding solar energy conversion efficiency was determined to peak at ca. 0.34% after 2 h of illumination. Recyclability tests revealed that the system can be used for stable  $\text{H}_2\text{O}_2$  generation for 5 cycles without any significant decay. Meanwhile, no detectable changes in the morphology and structure for the  $\text{NiFeO}_x/\text{BiVO}_4$  electrode (Fig. S16, ESI<sup>†</sup>), and no changes in the morphology of pTTh (Fig. S17, ESI<sup>†</sup>) were observed.

The produced alkali  $\text{HO}_2^-$  could be directly used in certain applications, for example, pulp and paper bleaching.<sup>42</sup> Of note, the produced  $\text{HO}_2^-$  is sufficiently concentrated to be applied in an  $\text{H}_2\text{O}_2$  fuel cell for electricity generation. With Ni foam as the anode and Prussian blue/carbon paper as the cathode, the  $\text{H}_2\text{O}_2$  fuel cell delivered an open circuit potential and a maximum power density of 0.6 V and  $2.7 \text{ mW cm}^{-2}$  (Fig. S18, ESI<sup>†</sup>), respectively. Combining the solar-driven  $\text{H}_2\text{O}_2$  production and the  $\text{H}_2\text{O}_2$  fuel cell for electricity generation is thus capable of addressing the intermittency of solar irradiation.

### Mechanistic understanding for $\text{O}_2$ activation

Photoelectrocatalysis is usually regarded as the light-excited electrocatalysis on a semiconducting photoelectrode.<sup>43,44</sup> To elucidate the role of light and identify the electrochemical behavior of pTTh, the electrochemical tests were carried out under identical conditions except that they were conducted in the dark. The results showed that the pTTh exhibits a similar  $2e^-$  selectivity of the electrocatalytic ORR in 0.1 M KOH to that under illumination (Fig. S19, ESI<sup>†</sup>). An early onset potential of 0.71 V relative to the  $2e^-$  pathway was observed with a low overpotential of 30 mV (Fig. S20, ESI<sup>†</sup>), although the current density was lower. Furthermore, a similar behavior of pH-dependence was found in which both the electrocatalytic activity and onset potential were enhanced with increasing pH (Fig. S21, ESI<sup>†</sup>). Meanwhile, the  $2e^-$  selectivity for  $\text{H}_2\text{O}_2$  production at different pH values remained almost the same between the PEC and electrochemical processes (Fig. S22, ESI<sup>†</sup>). Based on these results, it can be concluded that pTTh behaves indistinguishably when employed as an electrocatalyst or as a photoelectrode, with the selectivity primarily determined by the pH, independent of whether the electrode is driven by applied potential or light irradiation. Therefore, the electrochemical properties of pTTh are responsible for the high selectivity of  $\text{H}_2\text{O}_2$  generation in the basic environment.

We carried out density functional theory (DFT) calculations to gain insight into the mechanism and the high selectivity of the  $2e^-$  route in the electrochemical production of  $\text{H}_2\text{O}_2$  on pTTh in 0.1 M KOH solution. Preliminary calculations indicated that relative energies of the reaction intermediates with a

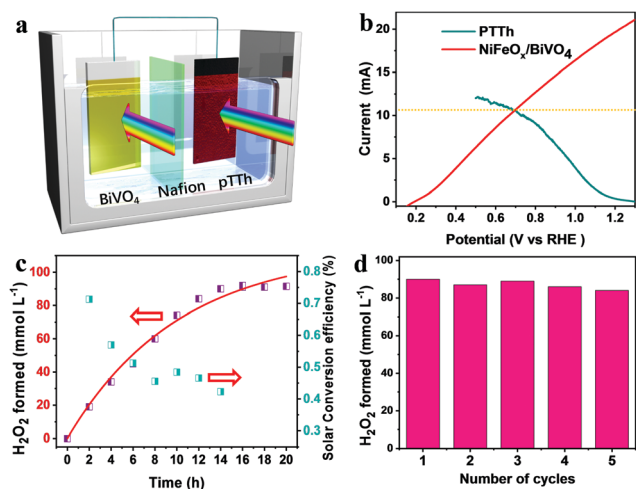


Fig. 5 (a) Illustration of the unbiased  $\text{H}_2\text{O}_2$  production device, with pTTh as the photocathode and  $\text{NiFeO}_x/\text{BiVO}_4$  as the photoanode in 0.1 M KOH and 1 M borate buffer electrolytes, respectively. The setup of the PEC cell is in parallel illumination mode. (b) Intersection of the  $\text{NiFeO}_x/\text{BiVO}_4$  photoanode and pTTh photocathode. (c) Time course for  $\text{H}_2\text{O}_2$  generation under simulated  $100 \text{ mW cm}^{-2}$  Xe illumination and corresponding solar-to- $\text{H}_2\text{O}_2$  efficiency. (d) Concentrations of  $\text{H}_2\text{O}_2$  produced with the two-electrode system during repeated operation cycles.

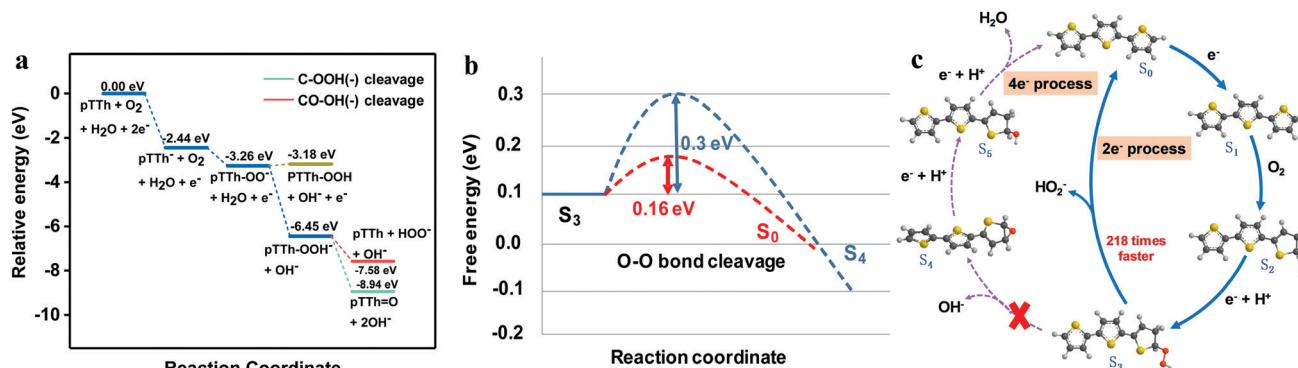


Fig. 6 (a) Energy profiles of key possible ORR pathways on pTTh (the energy profile for the overall mechanism is shown in Fig. S24, ESI†); (b) free energy diagram of the branching point for 2e<sup>-</sup> and 4e<sup>-</sup> selectivity of the ORR at pH = 13. The blue dashed line represents the O–O bond cleavage pathway, and the red dashed line represents the C–O bond cleavage. (c) Proposed reaction cycles of H<sub>2</sub>O<sub>2</sub> production with the energetically most feasible active sites. S<sub>0</sub> is the bare surface, S<sub>x</sub> (x = 1, 2, 3, 4, 5) are the structures of the intermediate states involved in the ORR. Red, gray, yellow and black balls represent oxygen, hydrogen, sulphur and carbon, respectively.

monomer of terthiophene (TTh) were similar to those with a dimer or a trimer of TTh. We used the monomer model (three thiophene rings) for the complete characterization of the reaction steps and the energy profile of the ORR for both thermodynamic and kinetic analysis. Note that the TTh and, for that matter, pTTh prefer a *trans* configuration in the orientation of the S atoms over a *cis* configuration. Fig. 6a shows the energy profile of the ORR derived from the Gibbs free energies of the proposed reaction steps (Table S2, ESI†) and Fig. 6c depicts the corresponding reaction steps. It was found that the binding of a dioxygen molecule to the neutral TTh is endothermic both in the gaseous phase and the aqueous phase, while attachment of an electron to TTh is exothermic by ~2.44 eV in an aqueous phase ( $\Delta G = \sim -2.44$  eV). Thus, reduction of pTTh *via* electron attachment to form the negative ion pTTh<sup>-</sup> is regarded as the first step (S<sub>0</sub> → S<sub>1</sub>). Addition of an O<sub>2</sub> molecule to the pTTh<sup>-</sup> leads to the formation of a peroxy anion pTTh–O<sub>2</sub><sup>-</sup> (S<sub>1</sub> → S<sub>2</sub>), a step that is exothermic by ~0.82 eV ( $\Delta G = \sim -3.26$  eV). The addition occurs at the  $\alpha$ -CH site of a terminal thiophene ring of TTh as the structure favors increased stabilization due to  $\pi$  electron conjugation effects (Fig. S23 and Table S3, ESI†). The peroxy anion abstracts a proton from a water molecule in the alkaline solution while accepting an electron in a proton-coupled step “pTTh–OO<sup>-</sup> + H<sub>2</sub>O + e<sup>-</sup> ⇌ pTTh–OOH<sup>-</sup> + OH<sup>-</sup>” (S<sub>2</sub> → S<sub>3</sub>) that is exothermic by ~3.19 eV and yields a stable intermediate, specifically a pTTh–OOH<sup>-</sup> species (relative energy  $\Delta G \sim -6.45$  eV). The next step is the cleavage of the CO–OH bond to evolve a hydroxide ion OH<sup>-</sup> (green lines) or cleavage of the C–OOH bond to evolve a peroxide ion HO<sub>2</sub><sup>-</sup> (red lines), which is the branching point for the 2e<sup>-</sup> and 4e<sup>-</sup> pathways (S<sub>3</sub> → S<sub>0</sub> for the 2e<sup>-</sup> route or S<sub>3</sub> → S<sub>4</sub> for the 4e<sup>-</sup> route). Either product requires one or more steps (protonation to form H<sub>2</sub>O<sub>2</sub> in the 2e<sup>-</sup> route or a reaction with H<sub>2</sub>O in the 4e<sup>-</sup> route). C–OOH bond cleavage leads to the recovery of the starting pTTh. In contrast, CO–OH bond cleavage results in the generation of epoxide pTTh=O which requires further reduction to evolve the second water molecule.

Both pathways of peroxide anion HO<sub>2</sub><sup>-</sup> formation and hydroxide anion OH<sup>-</sup> formation from the same pTTh–OOH<sup>-</sup> precursor are

thermodynamically favorable, exothermic by ~1.13 eV and ~2.49 eV, respectively. To establish selectivity required characterizing the kinetics of the two pathways, by determining the transition state structures (Fig. 6b) and applying transition state theory. The transition states (TS) for the C–OOH and CO–OH bond cleavage steps were characterized with the smaller basis set (cc-pVDZ). We then carried out single-point energy evaluations with the larger aug-cc-pVTZ basis set. We verified that the TS's have one and only one vibrational mode with an imaginary frequency (~330i cm<sup>-1</sup> for CO–OH cleavage and ~233i cm<sup>-1</sup> for C–OOH cleavage). At the TS for C–OOH cleavage, the C–OOH distance is ~1.82 Å while at the TS for CO–OH cleavage, the CO–OH distance is somewhat shorter ~1.74 Å. After correcting for zero-point vibrational energy, the energy barriers for the cleavage of C–OOH and CO–OH were determined to be ~+0.16 eV and ~+0.30 eV (Fig. 6b), respectively. According to transition state theory where the reaction rate  $k = A \exp(-\Delta G^*/k_B T)$  ( $\Delta G^*$  is the energy barrier), the reaction rate for peroxide ion formation (S<sub>3</sub> → S<sub>0</sub> with  $\Delta G^* \sim +0.16$  eV) is ~218 times faster than the rate for hydroxide ion formation (S<sub>3</sub> → S<sub>4</sub> with  $\Delta G^* \sim 0.30$  eV). Based on the above analysis, we proposed a reaction mechanism in which the 2e<sup>-</sup> pathway is kinetically favored over the 4e<sup>-</sup> pathway, leading to the high selectivity for H<sub>2</sub>O<sub>2</sub> production (Fig. 6c).

When considering the effects of pH on the energy profile, the relative energies associated with individual steps in Fig. 6a change only when the number of hydroxide ions changes in a given step. Step S<sub>3</sub> → S<sub>0</sub> conserves the number of hydroxide ions and pH does not affect its relative energy (exothermicity). In contrast, step S<sub>3</sub> → S<sub>4</sub> generates one extra hydroxide. The exothermicity of the step increases by  $\delta(\Delta E) \sim 2.3k_B T \times \delta(\text{pH})$  or  $\delta(\Delta E) \sim 0.059$  eV/(unit of pH). From the Bells–Evans–Polanyi rule, an increase in exothermicity leads to a decrease in energy barrier by about half of the increase in exothermicity. To lower the barrier of hydroxide formation (4e<sup>-</sup> pathway) by ~0.14 eV requires a change in pH of ~4.7 pH units. At pH ~ 9.3 the 4e<sup>-</sup> pathway would be predicted to be competitive with the 2e<sup>-</sup> pathway, and is then preferred at lower pH. This finding is broadly in accord with experiment, showing that the proposed

mechanism is consistent with the pH dependence observed experimentally.

## Conclusions

In summary, a metal-free organic polymer of pTTh enables the synthesis of solar H<sub>2</sub>O<sub>2</sub> in an efficient way by photoelectrochemical reduction of dissolved O<sub>2</sub> in alkaline solution. Under a constant bias of 0.65 V (vs. RHE) with visible light irradiation for 11 h, a H<sub>2</sub>O<sub>2</sub> concentration as high as 110 mmol L<sup>-1</sup> is achieved, which outperforms previously reported photosynthesis routes by ca. 2 orders of magnitude. Furthermore, a NiFeO<sub>x</sub>/BiVO<sub>4</sub> photoanode wired with the pTTh/CP photocathode enables the bias-free dual-photoelectrode synthesis of solar H<sub>2</sub>O<sub>2</sub> of concentration ~90 mmol L<sup>-1</sup> for several cycles without any noticeable decay. The high selectivity of the pTTh photoelectrode towards 2e<sup>-</sup> ORR originates from the intrinsic electrochemical properties of pTTh regardless of the incident light. Theoretical calculations suggest that the selectivity-determining step for the 2e<sup>-</sup> process is over ~200 times faster than that for the 4e<sup>-</sup> pathway. This study provides a green, low-cost and efficient route to synthesise H<sub>2</sub>O<sub>2</sub> from water, air and sunlight, which demonstrates promising generation of liquid solar fuel for future applications.

## Conflicts of interest

There are no conflicts of interest to declare.

## Acknowledgements

This work was financially supported by the DICP & QIBEBT (DICP&QIBEBT UN201709), and National Natural Science Foundation of China (No. 21573230, 51971094, 21761142018), and the National Key Research and Development Program of China (No. 2017YFA0204804, No. 2017YFB0102900), the Pioneer Initiative (B) Project of CAS (No. XDB17030200). XW and MD gratefully acknowledge partial start-up support from the University at Buffalo.

## References

- H. B. Gray, *Nat. Chem.*, 2009, **1**, 7.
- K. Dohyung, S. K. Kelsey, H. Dachao and Y. Peidong, *Angew. Chem., Int. Ed.*, 2015, **54**, 3259–3266.
- K. Sivula and R. van de Krol, *Nat. Rev. Mater.*, 2016, **1**, 15010.
- J. L. White, M. F. Baruch, J. E. Pander, Y. Hu, I. C. Fortmeyer, J. E. Park, T. Zhang, K. Liao, J. Gu, Y. Yan, T. W. Shaw, E. Abelev and A. B. Bocarsly, *Chem. Rev.*, 2015, **115**, 12888–12935.
- E. V. Kondratenko, G. Mul, J. Baltrusaitis, G. O. Larrazábal and J. Pérez-Ramírez, *Energy Environ. Sci.*, 2013, **6**, 3112–3135.
- J. H. Kim, D. Hansora, P. Sharma, J.-W. Jang and J. S. Lee, *Chem. Soc. Rev.*, 2019, **48**, 1908–1971.
- S. Kato, J. Jung, T. Suenobu and S. Fukuzumi, *Energy Environ. Sci.*, 2013, **6**, 3756–3764.
- Y. Jiang, P. Ni, C. Chen, Y. Lu, P. Yang, B. Kong, A. Fisher and X. Wang, *Adv. Energy Mater.*, 2018, **8**, 1801909.
- K. Sayama, *ACS Energy Lett.*, 2018, **3**, 1093–1101.
- X. Shi, S. Siahrostami, G.-L. Li, Y. Zhang, P. Chakthranont, F. Studt, T. F. Jaramillo, X. Zheng and J. K. Nørskov, *Nat. Commun.*, 2017, **8**, 701.
- C. Xia, Y. Xia, P. Zhu, L. Fan and H. Wang, *Science*, 2019, **366**, 226–231.
- S. A. Mousavi Shaegh, N.-T. Nguyen, S. M. Mousavi Ehteshami and S. H. Chan, *Energy Environ. Sci.*, 2012, **5**, 8225–8228.
- J. M. Campos-Martin, G. Blanco-Brieva and J. L. G. Fierro, *Angew. Chem., Int. Ed.*, 2006, **45**, 6962–6984.
- J. H. Baek, T. M. Gill, H. Abroshan, S. Park, X. Shi, J. Nørskov, H. S. Jung, S. Siahrostami and X. Zheng, *ACS Energy Lett.*, 2019, **4**, 720–728.
- H. Dotan, K. Sivula, M. Grätzel, A. Rothschild and S. C. Warren, *Energy Environ. Sci.*, 2011, **4**, 958–964.
- S. Siahrostami, G.-L. Li, V. Viswanathan and J. K. Nørskov, *J. Phys. Chem. Lett.*, 2017, **8**, 1157–1160.
- K. Fuku and K. Sayama, *Chem. Commun.*, 2016, **52**, 5406–5409.
- M. Teranishi, S.-i. Naya and H. Tada, *J. Am. Chem. Soc.*, 2010, **132**, 7850–7851.
- H.-i. Kim, O. S. Kwon, S. Kim, W. Choi and J.-H. Kim, *Energy Environ. Sci.*, 2016, **9**, 1063–1073.
- Y. Kofuji, Y. Isobe, Y. Shiraishi, H. Sakamoto, S. Tanaka, S. Ichikawa and T. Hirai, *J. Am. Chem. Soc.*, 2016, **138**, 10019–10025.
- A. J. Hoffman, E. R. Carraway and M. R. Hoffmann, *Environ. Sci. Technol.*, 1994, **28**, 776–785.
- M. Jakešová, D. H. Apaydin, M. Sytnyk, K. Oppelt, W. Heiss, N. S. Sariciftci and E. D. Głowacki, *Adv. Funct. Mater.*, 2016, **26**, 5248–5254.
- K. Mase, M. Yoneda, Y. Yamada and S. Fukuzumi, *Nat. Commun.*, 2016, **7**, 11470.
- S. Ghosh, N. A. Kouamé, L. Ramos, S. Remita, A. Dazzi, A. Deniset-Besseau, P. Beaunier, F. Goubard, P.-H. Aubert and H. Remita, *Nat. Mater.*, 2015, **14**, 505.
- B. Zhang, S. Wang, W. Fan, W. Ma, Z. Liang, J. Shi, S. Liao and C. Li, *Angew. Chem., Int. Ed.*, 2016, **55**, 14748–14751.
- B. Zhang, L. He, T. Yao, W. Fan, X. Zhang, S. Wen, J. Shi and C. Li, *ChemSusChem*, 2019, **12**, 1026–1032.
- B. Kolodziejczyk, O. Winther-Jensen, D. R. MacFarlane and B. Winther-Jensen, *J. Mater. Chem.*, 2012, **22**, 10821–10826.
- S. Fukuzumi, Y.-M. Lee and W. Nam, *Chem. – Eur. J.*, 2018, **24**, 5016–5031.
- B. Zhang, W. Fan, T. Yao, S. Liao, A. Li, D. Li, M. Liu, J. Shi, S. Liao and C. Li, *ChemSusChem*, 2017, **10**, 99–105.
- K. Schwinghammer, M. B. Mesch, V. Duppel, C. Ziegler, J. Senker and B. V. Lotsch, *J. Am. Chem. Soc.*, 2014, **136**, 1730–1733.
- Q. Li, B. W. Noffke, Y. Wang, B. Menezes, D. G. Peters, K. Raghavachari and L.-S. Li, *J. Am. Chem. Soc.*, 2014, **136**, 3358–3361.
- K. J. J. Mayrhofer, D. Strmcnik, B. B. Blizanac, V. Stamenkovic, M. Arenz and N. M. Markovic, *Electrochim. Acta*, 2008, **53**, 3181–3188.
- H. Wang, Y. Liang, Y. Li and H. Dai, *Angew. Chem., Int. Ed.*, 2011, **50**, 10969–10972.

- 34 J. Weinstein and B. H. J. Bielski, *J. Am. Chem. Soc.*, 1979, **101**, 58–62.
- 35 G.-h. Moon, W. Kim, A. D. Bokare, N.-e. Sung and W. Choi, *Energy Environ. Sci.*, 2014, **7**, 4023–4028.
- 36 S. Zhao, X. Zhao, H. Zhang, J. Li and Y. Zhu, *Nano Energy*, 2017, **35**, 405–414.
- 37 T. W. Kim and K.-S. Choi, *Science*, 2014, **343**, 990–994.
- 38 S. Ye, C. Ding, R. Chen, F. Fan, P. Fu, H. Yin, X. Wang, Z. Wang, P. Du and C. Li, *J. Am. Chem. Soc.*, 2018, **140**, 3250–3256.
- 39 K. Yongbo, J. Qingxin, N. Hiroshi, Y. Taro, K. Akihiko and D. Kazunari, *Adv. Energy Mater.*, 2016, **6**, 1501645.
- 40 L. Pan, J. H. Kim, M. T. Mayer, M.-K. Son, A. Ummadisingu, J. S. Lee, A. Hagfeldt, J. Luo and M. Grätzel, *Nat. Catal.*, 2018, **1**, 412–420.
- 41 J. H. Kim, J.-W. Jang, Y. H. Jo, F. F. Abdi, Y. H. Lee, R. van de Krol and J. S. Lee, *Nat. Commun.*, 2016, **7**, 13380.
- 42 J. M. Campos-Martin, G. Blanco-Brieva and J. L. G. Fierro, *Angew. Chem., Int. Ed.*, 2006, **45**, 6962–6984.
- 43 D. Li, J. Shi and C. Li, *Small*, 2018, **14**, 1704179.
- 44 E. Pastor, F. L. Formai, M. T. Mayer, S. D. Tilley, L. Francàs, C. A. Mesa, M. Grätzel and J. R. Durrant, *Nat. Commun.*, 2017, **8**, 14280.